Cation partitioning of garnets from Sittampundi granulite: Their petrogenetic implications

Sachinath Mitra[1] and Maibam Bidyananda[2,*]

[1]Department of Geological Sciences, Jadavpur University, Kolkata 700 032, India
[2]Department of Geological Sciences, Gauhati University, Guwahati 781 014, India

Garnets from high *P–T* granulite fields of Sittampundi (South India) were investigated by ^{57}Fe Mössbauer spectroscopy and electron microprobe analysis. The room-temperature three-band spectra which have been split into two doublets, revealed Fe^{2+} ions to be exclusively located at the dodecahedral site (isomer shift = 1.303–1.389 mm/s; quadrupole splitting (QS) = 3.423–3.822 mm/s) and Fe^{3+} ions at tetrahedral site (isomer shift = 0.006–0.163 mm/s; QS = 0.520–0.663 mm/s). The octahedral site was completely free from both these ions. $Fe^{3+}/\sum Fe$ varying between 0.073 and 0.150, and the presence of octahedral Si indicate that the studied garnet formation lies in high *P–T* field. The high values of QS for tetrahedral Fe^{3+} suggest that the occupied site is regular with little distortion. The fairly broad linewidth, 0.455–0.596 mm/s of Fe^{3+} doublet may arise from a substitution of some tetrahedral Si by the $(OH)^{-1}$ group. The strong partition and ordering of Fe^{2+} and Fe^{3+} in dodecahedral and tetrahedral sites, leaving the octahedral site totally free from iron suggest slow cooling and recrystallization of garnet at high temperature.

Keywords: Garnets, majorite, Mössbauer spectroscopy, octahedral silicon, Sittampundi granulite.

THE garnet group of minerals (cubic with space group *Ia3d*) occurs commonly in metamorphic as well as in high-pressure igneous rocks and detrital grains in sediments. The general formula of garnet is $\{X_3\}[Y_2](Z_3)O_{12}$ where { }, [ ] and ( ) denote eightfold, sixfold and fourfold coordination sites respectively (notation after Geller[1]); X = Mg, Mn, Fe^{2+} and Ca; Y = Fe^{3+}, Ti, Cr and Al, and Z = Si and Al. Winchell[2] compositionally divided garnets into pyralspite (pyrope, almandine, spessartine) and ugrandite (uvarovite, grossular, andradite) series. Miscibility between these two series is limited, but within them substitution is extensive. The structure of garnet (nesosilicate) consists of alternating ZO_4 tetrahedra and YO_6 octahedra, which share corners to form a three-dimensional framework. The divalent ions (X) surrounded by eight oxygens occur in the interstices within the Si–Al network and the coordination polyhedra have the shape of a distorted cube, often described as triangular dodecahedron.

*For correspondence. (e-mail: bmaibam@yahoo.com)

Mössbauer spectroscopy of Fe-bearing garnets provides crystal chemical information by revealing the site occupancy and valence state of iron. As cation distributions are sensitive to varying *P–T* conditions, the distribution of cations between different sites has important implications for obtaining the thermal history of rocks[3–5]. Several Mössbauer spectroscopic studies of garnets have been carried out[6–9]. Amthauer *et al.*[6] reported ranges in hyperfine parameters corresponding to dodecahedrally and tetrahedrally coordinated Fe^{2+} and octahedrally and tetrahedrally coordinated Fe^{3+}. Details of the coordination sites of Fe atoms in crystal lattice can also be assessed from the calculated hyperfine parameters. The aim of the present study is to distribute the cations in different sites of natural garnet samples using ^{57}Fe Mössbauer spectroscopic and electron microprobe analysis (EMPA) studies. The result would have important implications for the crystallochemical behaviour of garnets at high pressure and temperature condition.

The Sittampundi Anorthosite Complex occurs as a layered igneous body. The area forms a part of the granulite terrain of South India. Major rock types are chromitite-bearing meta-anorthosite, amphibolite, basic granulite, two-pyroxene granulite, leptynite, biotite gneiss and pink granite. In this complex, amphibolite and chromitite occur as small discontinuous bands/lenses within meta-anorthosite. Basic granulite occurs as discontinuous but conformable layers within meta-anorthosite. Two-pyroxene granulite and pink granite occurring within the biotite gneiss constitute the later intrusive phases[10]. EMPA analyses were carried out in garnets separated from basic granulite, two pyroxene granulite, leptynite and meta-anorthosite in different areas of the Sittampundi complex. However, garnets from the basic granulite in different areas of the Sittampundi complex were studied using Mössbauer spectroscopy. Two samples were collected from a spot between Sittampundi and Nallakvundanpam (11b, 12c), another from southwest of Marappampalaiyam (33) and the fourth one from east of Pudor (36a). A brief geological description of the studied area is presented elsewhere[11].

EMPA analyses of the samples were carried out using a JEOL-733 superprobe (wavelength dispersive method) at the Department of Geology, Yonsei University, Seoul, using an acceleration voltage of 15 kV with beam current of 10 nA and 2 μm beam diameter. Average spectrum counts were compared with natural standards and data were reduced using the Bence and Albee method[12]. For Mössbauer analyses, garnet grains from sieved samples were handpicked using the microscope. The purity of the selected grains was checked by X-ray diffractometry (XRD) and was found to be of pure garnet. The calculated cell edge is presented in Table 1. Mössbauer spectra were recorded at room temperature (298 K) using 10 mCi (^{57}Co/Rh) source with a constant acceleration drive. The finely powdered samples were pressed tight in plexi

holders and based on the iron content (known from EMPA) determined amounts (for instance, for sample 36a, the amount was 68 mg) were taken to optimize the thickness effect. The spectra were fitted with Lorentzian lines using a nonlinear least square fit program. For each doublet the intensity and line width were constrained to be equal. The velocity calibration was performed with respect to pure metallic iron (99.99%).

Table 1. Relation between cell edge (Å) and $Fe^{3+}/\Sigma Fe$ in Sittampundi garnet

Sample	a_0 (Å)	$Fe^{3+}/\Sigma Fe$
11b	11.601	0.150
12c	11.509	0.073
33	11.669	0.147
36a	11.609	0.081

Table 2. Representative chemical analysis of the studied garnets

Oxide	1	12b	13
SiO_2	38.85	39.00	39.66
TiO_2	0.02	0.59	0.08
Cr_2O_3	0.12	–	0.02
Al_2O_3	21.31	17.61	21.78
FeO*	29.61	8.62	22.50
MnO	0.52	0.30	1.20
MgO	8.34	0.54	8.53
NiO	–	–	0.03
CaO	1.11	32.65	6.58
Na_2O	–	–	0.08
K_2O	–	0.01	0.03
Total	99.88	99.32	100.49
Cations in garnet calculated on 24 oxygen basis			
Si	6.040	6.106	6.036
Ti	0.002	0.070	0.009
Cr	0.015	–	0.002
Al	3.905	3.250	3.907
Fe	3.850	1.128	2.864
Ni	–	–	0.004
Mn	0.068	0.040	0.155
Mg	1.933	0.126	1.935
Ca	0.185	5.478	1.073
Na	–	–	0.024
K	–	0.002	0.006
Total	15.998	16.200	16.015
X_{Mg}	0.334	0.147	0.403
Fe^{2+}**	n.d.	0.365	2.864
Fe^{3+}**	n.d.	0.199	0.001
End-members (%)			
Pyrope	32.02	1.86	32.10
Almandine	63.78	16.66	47.53
Spessartine	1.13	0.59	2.57
Grossular	3.07	80.89	17.80

*Total iron expressed as FeO; **Stoichiometrically determined from microprobe analysis $Fe^{3+} = 8-2Si-2Ti-Al-Cr$ (ΣCations = 8; ΣOxygen = 12) from Ryburn *et al.*[33]; n.d., Negative values of Fe^{3+}.

Garnets in Sittampundi granulitic rocks are primarily almandine–pyrope solid-solution with some grossular and spessartine component (Tables 2 and 3). The end-members of some garnets in basic granulite were rich in almandine component ($Alm_{49.7-56.96}Pyr_{9.8-32.72}Gro_{15.41-38.17}Spess_{0.12-2.18}$), while others were rich in pyrope component ($Alm_{22.67-41.21}Pyr_{43.05-59.58}Gro_{12.94-19.89}Spess_{0.07-1.07}$). The end-member components in two-pyroxene granulite, leptynite and meta-anorthosite were $Alm_{47.52}Pyr_{32.10}Gro_{17.80}Spess_{2.57}$, $Alm_{63.78}Pyr_{32.02}Gro_{3.07}Spess_{1.13}$ and $Alm_{16.66}Pyr_{1.86}Gro_{80.89}Spess_{0.59}$ respectively.

X_{Mg} of garnets in basic granulites ranged between 0.158 and 0.724, whereas in two-pyroxene granulite, leptynite and meta-anorthosite these were 0.403, 0.334 and 0.147

Table 3. Average chemical analysis and cation distribution of garnet from EMPA and Mössbauer studies

Oxide	11b	12c	33	36a
SiO_2	39.20	40.63	38.66	38.75
TiO_2	0.08	0.06	0.12	0.02
Cr_2O_3	0.09	0.03	0.02	–
Al_2O_3	21.32	22.54	20.92	21.08
FeO	20.53	16.75	19.80	24.58
Fe_2O_3	4.03	1.47	3.79	2.42
MnO	0.78	0.33	0.67	0.71
MgO	6.40	13.00	3.03	6.59
NiO	–	0.01	–	–
CaO	8.52	5.30	13.14	6.28
Na_2O	0.02	0.03	0.02	0.02
K_2O	–	0.01	–	0.01
Total	100.97	100.16	100.17	100.46
Cations in garnet calculated on 24 oxygen basis				
Si^{IV}	5.534	5.836	5.553	5.716
Fe^{3+}	0.466	0.164	0.447	0.284
Al^{IV}	–	–	–	–
Si^{VI}	0.500	0.197	0.509	0.310
Al^{VI}	3.868	3.944	3.868	3.861
Ti	0.009	0.004	0.014	0.002
Cr	0.012	0.004	0.003	–
Ni	–	0.001	–	–
Fe^{2+}	2.644	2.076	2.596	3.200
Mn	0.102	0.045	0.085	0.093
Mg	1.471	2.874	0.706	1.523
Ca	1.407	0.839	2.204	1.046
Na	0.005	0.009	0.006	0.005
K	–	0.002	–	0.002
Total	16.018	15.995	15.991	16.042
X_{Mg}	0.358	0.581	0.214	0.323
Fe^{3+}/Fe^{2+}*	0.176	0.079	0.172	0.089
End-members (%)				
Pyrope	26.16	49.26	12.63	25.98
Almandine	47.01	35.59	46.43	54.59
Spessartine	1.81	0.77	1.52	1.59
Grossular	24.70	14.28	39.33	17.84
Uvarovite	0.32	0.10	0.09	–

*From Mössbauer spectra taken at room temperature.

Table 4. Variational range of $[Al]^{IV}$, $[Al]^{VI}$, Ca, Na, TiO_2 and Cr_2O_3 of the studied garnets

Rock type	$[Al]^{IV}$	$[Al]^{VI}$	Ca	Na	TiO_2	Cr_2O_3
Basic granulite	0.000–0.078	3.640–4.000	0.783–2.271	0.000–0.034	0.00–0.12	0.00–0.13
Two-pyroxene granulite	–	3.907	1.073	0.024	0.08	0.02
Leptynite	–	3.905	0.185	–	0.02	0.12
Meta-anorthosite	–	3.250	5.478	–	0.59	–

Table 5. Mössbauer parameters of garnet with $Fe^{3+}/\sum Fe$ ratios and chi-square of the fitting

Sample no.	Isomer Shift (IS) (mm/s)	Quadrupole splitting (QS) (mm/s)	Distribution			Width (mm/s)	Area (%)	χ^2	$Fe^{3+}/\sum Fe$
			Dodecahedral	Octahedral	Tetrahedral				
11b	1.303	3.423	Fe^{2+}			0.308	85.00	1.40	0.150
	0.153	0.614			Fe^{3+}	0.455	15.00		
12c	1.320	3.441	Fe^{2+}			0.303	92.70	1.22	0.073
	0.050	0.663			Fe^{3+}	0.596	7.30		
33	1.334	3.490	Fe^{2+}			0.313	85.30	1.38	0.147
	0.163	0.520			Fe^{3+}	0.517	14.70		
36a	1.398	3.822	Fe^{2+}			0.309	91.85	1.32	0.081
	0.006	0.630			Fe^{3+}	0.484	8.15		

respectively. In garnet the $[Al]^{IV}$, $[Al]^{VI}$, Ca and Na contents were strongly influenced by temperature and pressure at the time of crystallization[13]. In Sittampundi garnets, their contents are as given in Table 4 (cation calculation based on 24 oxygen basis).

Sittampundi garnets show low TiO_2 and Cr_2O_3 content, with a little tetrahedral Al, except in a few samples. For a given whole-rock composition, garnets contain higher Ca with increasing pressure at constant temperature[14,15]. Analogous to Al, Cr partitions preferentially into garnet in relation to the coexisting orthopyroxene when the temperature decreases and pressure increases[16]. Presence of low Cr content in Sittampundi garnets with variable amounts of Ca corresponds to Ca enrichment in garnet with decreasing temperature of formation of the garnet. This Ca enrichment correlates well with the isobaric cooling of the granulitic metamorphism relating garnet crystallization at high depths under the crust.

The room-temperature Mössbauer spectra of the garnets (Figure 1) show two asymmetric peaks in the paramagnetic doublet, with a more intense peak at lower velocity region for samples 11b, 12c and 33; but it is reverse for sample 36a. Asymmetry in the quadrupole doublet in the room-temperature garnet spectra can be explained as arising out of paramagnetic relaxation of Fe^{2+} ions in the 24c position[6,7,17]. No dependence of this asymmetry on garnet composition has been noted within the pyrope–almandine series, suggesting that this is not due to the next nearest neighbour (NNN) effects[18]. However, no statistically significant asymmetry is always apparent between the low and high velocity peaks in natural garnets[9].

In the present case, fitting of the Mössbauer spectra of all the studied samples was approached by two doublet fits (Fe^{2+} and Fe^{3+} doublets only), following some early workers. The determined hyperfine parameters (e.g. isomer shift (IS), quadrupole splitting (QS)), line widths and chi-square values are within the acceptable limits. The Mössbauer parameters as well as the assignment of iron doublet of a particular crystallographic site are presented in Table 5. The most intense doublet with the isomer shift (IS) 1.303 mm/s (for sample 11b), 1.320 mm/s (for sample 12c), 1.334 mm/s (for sample 33), 1.389 mm/s (for sample 36a) and corresponding QS, i.e. 3.423, 3.441, 3.490 and 3.822 mm/s were assigned to Fe^{2+} in eightfold coordinated site[6,9,19]. The QS value of sample 36a is larger than that reported by early workers and might be due to high almandine component (Table 6)[7].

In garnet, at 77 K IS of 0.04–0.13 mm/s and QS of 0.71–1.01 mm/s were assigned[20] to tetrahedral Fe^{3+}. At 77 K, Fe^{3+} in octahedral coordination had[6,17] IS range of 0.391–0.602 mm/s and QS 0.211–0.640 mm/s (see Table 6), but at 298 K Fe^{3+} in octahedral coordination had[17,21] IS range of 0.391–0.602 mm/s (see Table 6). The predominant site for Fe^{3+} changes from tetrahedral to octahedral at $Fe^{3+}/\sum Fe \sim 0.09$ in garnet[8]. There is also a marked difference in the position of the low-velocity peak of the Fe^{3+} doublet[20], which is at lower velocity in the presence of tetrahedral Fe^{3+} than the octahedral Fe^{3+}. In the present case the doublet showing IS of 0.153 mm/s (for sample 11b), 0.05 mm/s (for sample 12c), 0.163 mm/s (for sample 33), 0.006 mm/s (for sample 36a) and corresponding QS of 0.614, 0.663, 0.520, 0.630 mm/s with $Fe^{3+}/\sum Fe$ ratios within 0.0.073–0.150 mm/s could be assigned to Fe^{3+} in tetrahedral site.

In general, the $Fe^{3+}/\sum Fe$ values in garnet increase with increasing pressure and temperature and the coordination

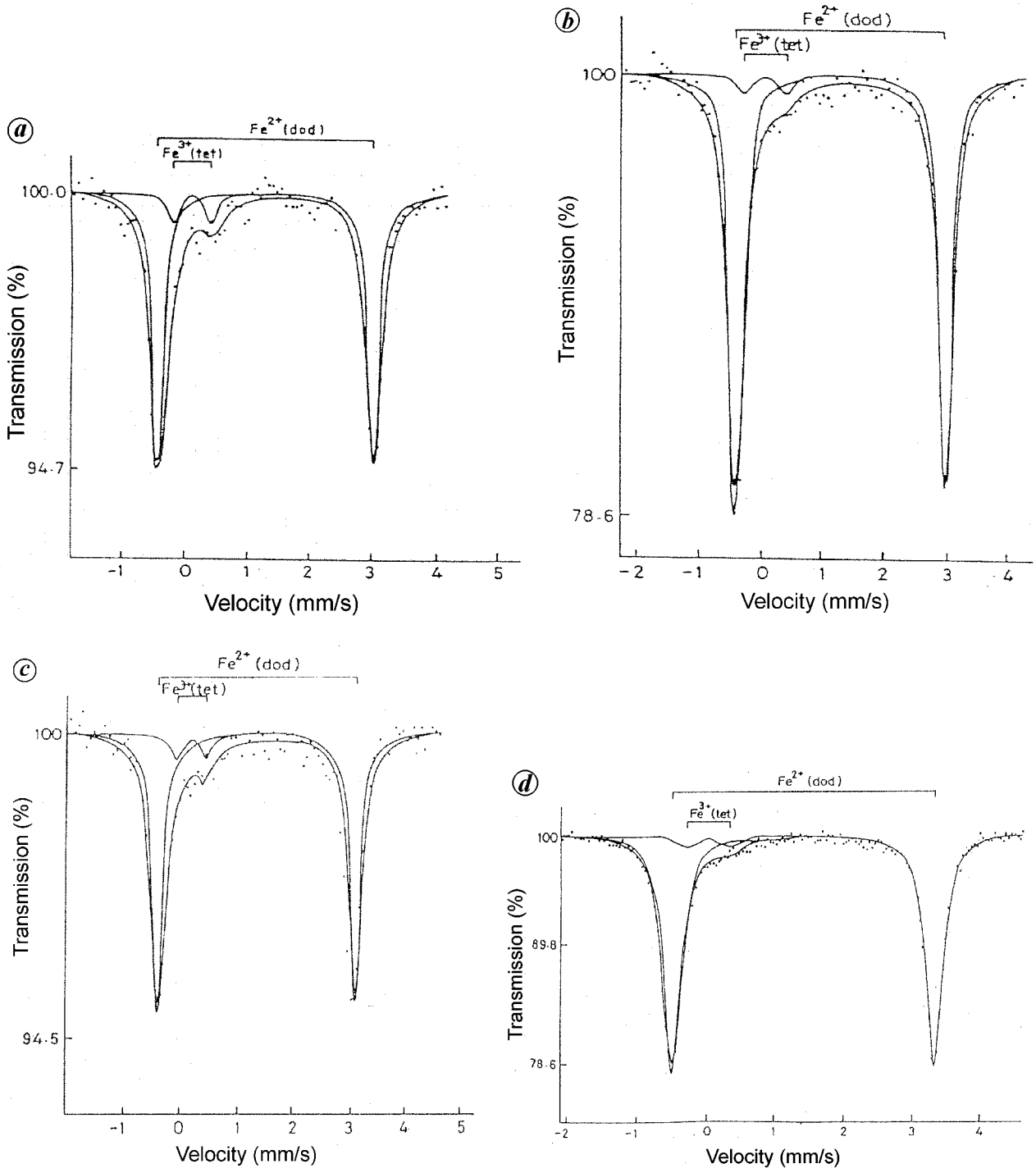

Figure 1. Room temperature ^{57}Fe Mössbauer spectra of garnets from basic granulite. ***a***, Sample 11b; ***b***, Sample 12c; ***c***, Sample 33 and ***d***, Sample 36a.

state of Fe^{3+} correlates positively with pressure[20]. Garnets in xenoliths[8] derived from <50 kb contain tetrahedral Fe^{3+} and those derived from >50 kb contain octahedral Fe^{3+}. The low-*T*, lower Fe^{3+} garnets have $Fe^{3+}/\sum Fe$ varying from 0.048 to 0.057, but the high-*T* lherzolites contain garnets with $Fe^{3+}/\sum Fe$ varying from 0.107 to 0.118, with the highest *P*, *T* sample[17] containing the most of Fe^{3+}. The $Fe^{3+}/\sum Fe$ ratios of the Sittampundi garnets vary between 0.073 and 0.150, which indicates its formation at high pressure–temperature conditions. It is incorrect to correlate the $Fe^{3+}/\sum Fe$ of the garnets directly with the fO_2 of the source region, and one can conclude that the high Fe^{3+} garnets were derived from a more oxidized region than the low Fe^{3+} garnets[17]. Accordingly, the decreasing order of

Table 6. Mössbauer parameters of garnet reported by early workers and the present work

Reference	Temperature (K)	IS (mm/s)	QS (mm/s)	Distribution		
				Dodecahedral	Octahedral	Tetrahedral
Natural garnet						
6	77	1.33–1.44	3.55–3.73	Fe^{2+}		
		0.42–0.52	0.26–0.64		Fe^{3+}	
7 (Alm_{86})	294	1.25–1.31	3.51–3.54	Fe^{2+}		
	78	1.42	3.66	Fe^{2+}		
	4.2	1.27–1.35	3.41–3.84	Fe^{2+}		
21 (almandines)	298	1.31–1.42	3.52–3.63	Fe^{2+}		
		0.27–0.48	0.24–0.28		Fe^{3+}	
17	298	1.27–1.31	3.50–3.62	Fe^{2+}		
		0.28–0.41	0.15–0.36		Fe^{3+}	
Present work	298	1.30–1.40	3.42–3.82	Fe^{2+}		
		0.01–0.16	0.52–0.66			Fe^{3+}
Synthetic garnet						
7 (Alm_{100})	295	1.27–1.30	3.50–3.54	Fe^{2+}		
	78	1.42	3.67	Fe^{2+}		
	11	1.42	3.65	Fe^{2+}		
	4.2	1.23–1.39	3.57–4.02	Fe^{2+}		
16	298	1.28	3.61	Fe^{2+}		
		0.19	0.42		Fe^{3+}	
9	298	1.30	3.50	Fe^{2+}		
		0.32–0.40	0.21–0.55		Fe^{3+}	
	80	1.43	3.70	Fe^{2+}		
		0.34–0.48	0.11–0.51		Fe^{3+}	

the Sittampundi garnet in relation to the fO_2 of the source region was 11b > 33 > 36a > 12c. According to Woodland and Wood[21], the higher cell edge garnets are more oxidized and Fe^{3+} is largely responsible for the larger cell edges of the same almandines, although Fe^{3+} has less ionic radius than the Fe^{2+} ion. This happens because of the presence of accompanying vacancy generated for charge balance in the process of oxidation of Fe^{2+} to Fe^{3+}. In case of Sittampundi garnets, the relation between cell edge and Fe^{3+} contents is given in Table 1.

Although $Fe^{3+}/\sum Fe$ ranges between 0.073 and 0.150, no molecule of skiagite (obsolete nomenclature for $Fe_3^{2+}Fe_2^{3+}Si_3O_{12}$)[9] is conceived to be present in the Sittampundi samples. It is because whatever Fe^{3+} is present, is located exclusively at the tetrahedral site and none at all in the dodecahedral or octahedral sites. This yields[9] a strong Fe^{3+} doublet with centre shift (CS) of 0.32–0.40 mm/s. The high values of QS (0.520–0.663 mm/s) of the tetrahedral Fe^{3+} in our sample also suggest that the site is regular, with little distortion. The high values of Fe^{3+} calculated from the spectral measure may also arise out of the high recoil-free fraction (f) which is dependent on, among many other factors, the crystal site and the bonding (M–O). Greater ionicity in bonding leads to greater values of f.

The fairly broad line width (FWHM) of 0.455–0.596 mm/s for the Fe^{3+} doublet may also be due to the presence of different arrangements of next nearest neighbours; the line broadening is due to the substitution of Si^{4+} by $(OH)^{-1}$ group on some tetrahedral sites[9]. The classical way to incorporate H_2O or $(OH)^-$ into the garnet structure is by substituting Si^{4+} with $4H^+$ or $(SiO_4)^{4-}$ with $4(OH)^-$, as shown by neutron diffraction[22]. This means that a vacant Si^{4+} site has to be occupied by $4H^+$ in order to charge balance. In major mineral phases of mantle xenoliths, variable amounts of structural water occur as defects. The solubility of water in olivine from mantle xenoliths increases rapidly with pressure, reaching a maximum value near 0.12 wt% at a temperature of 1100°C at pressures corresponding to 400 km depth[23]. The IR spectral study conclusively shows the $(OH)^{-1}$ bands (3700–3200 cm^{-1}) in these samples[24]. The structural unit of dodecahedra and tetrahedra surrounding the octahedral site in garnet forms a distorted trigonal antiprism and the environment about Fe^{3+} ion never has perfect cubic symmetry. Changes in the dodecahedral site occupancy with composition will influence the electric field gradient (EFG), leading to a change in the Fe^{3+} QS. The high QS values (0.520–0.663 mm/s) of the Fe^{3+} state observed in Sittampundi samples represent such an influence of strong EFG around it. The field gradient at the tetrahedral site is considerably larger than at the octahedral site, thus lending support to the suggestion that the electron density distribution of the tetrahedrally coordinated polyhedra in an-

dradite and grossular should be considered strongly distorted. In silicate garnets, EFG at the octahedral sites is generally positive; in rare garnets it is negative[20]. It is significant that the dodecahedral site is exclusively occupied by Fe^{2+} iron with some Fe^{3+}; whereas the octahedral site is completely free from both these ions. This strong partitioning and ordering of Fe^{2+} and Fe^{3+} in dodecahedral and tetrahedral sites suggest slow cooling and recrystallization of garnet at high temperature. The thermometry of garnet–clinopyroxene indicates the temperature to be 950–750°C (at a pressure of 10–7 kb from core to rim compositions). It should be emphasized that no study of natural samples from high *P–T* field has been made earlier revealing such a kind of complete ordering of Fe^{2+} at the dodecahedral site and Fe^{3+} at the tetrahedral site, while leaving the octahedral site completely free of iron. The Sittampundi garnet crystallized at high *P–T* condition followed by a slow process of cooling (6°C/Ma)[25]. It attained perfect ordering as manifested by the absence of any indication of residual strain or structural distortion of the sites and consequent changes in bond length, bond angle distortion. These could have been manifested by developing anisotropism, birefringence, anomalous extinction, etc.[26,27], which are not observed optically.

In Sittampundi garnets the dodecahedral site is occupied by Fe^{2+} and tetrahedral site by Fe^{3+}, but in the Mössbauer spectra there is no evidence of electron-hopping between these two sites at room temperature. Evidently, electron transfer between Fe^{2+} and Fe^{3+} in these two sites is not possible. This again suggests that the polyhedra at these two sites neither share common faces nor edges. Absence of Fe^{2+} and Fe^{3+} at octahedral sites obstructs the generation of polarons. None of the iron nuclei at these sites 'see' the electron-hopping to generate any additional line in the Mössbauer spectra taken at room temperature.

Enstatite and diopside manifest a solubility in garnet at higher pressure[28] and pyroxene would disappear at depths of about 540 km and get replaced by a complex garnet solid solution (cf. majorite). Textural types (triangular network) of exsolved pyroxene within garnet as a result of pressure release are commonly seen in the transition zone. When the clinopyroxene component is recombined with the host garnet's composition, a garnet with excess Si is produced. The Si/Al atomic ratios of these garnets were similar to those of garnets associated with kimberlites, formed at great depths. This excess Si is in octahedral coordination (Si^{VI}) and is associated with an Al^{VI} deficit (unbalanced by Cr and Ti), which typifies the chemical signature of pyroxene component dissolved in the garnet structure. The presence of Na may substantially expand the stability field of high-Si garnets to lower pressure. Northern Lesotho xenolith data[29] indicate evidence of incipient pyroxene solid solutions in garnets as indicated by excess Si of up to 0.038 over the stoichiometric value of 3.000. Since Ti probably replaces Si in the garnet lattice, it could be argued that the (Si + Ti) value is a more significant measurement; and in this case, for which a maximum of 3.081 or 2.71% above stoichiometry is attained[30].

Except those present in some basic granulite, other Sittampundi garnets have excess Si over the stoichiometric value of 6.000 at the tetrahedral site (cation calculation on 24 oxygen basis). Presence of tetrahedral Fe^{3+} in garnet from Mössbauer study strongly depicts the existence of octahedral Si from oversaturation of the tetrahedral site (Table 3). Octahedral Si in garnet of Sittampundi complex suggests that a complete re-equilibration of garnet after its formation was not possible because of the syntectonic decompression process affecting the complex. Some thin exsolution lamellae are common in garnet of basic granulite, two-pyroxene granulite and leptynite of this complex.

The present Mössbauer study on four natural garnet samples from the basic granulite of the Sittampundi complex shows that Fe^{3+}, Al^{3+} and Fe^{2+} along with Ca^{2+} are exclusively located at tetrahedral, octahedral and dodecahedral sites respectively. This partition and ordering of Fe^{3+} and Fe^{2+} implies a slow cooling and recrystallization of garnet under high temperature and pressure conditions (950–750°C and 10–7 kb). The $Fe^{3+}/\sum Fe$ ratios varying between 0.073 and 0.150 also indicate formation at higher pressure and temperature conditions. Sittampundi garnets have excess Si over the stoichiometric value of 6.000 at the tetrahedral site (calculated on 24 oxygen basis) and the presence of tetrahedral Fe^{3+} strongly depicts the existence of octahedral Si on oversatuation of all tetrahedral sites by silicon. When garnet forms a solid solution with orthopyroxene under pressure, $2Al \Leftrightarrow Mg, Si$ replacement occurs successively in an octahedral site and the total amount of Si exceed a value of 6 (24 oxygen basis)[31].

We are not sure at this point of our observation whether the stability field of high-Si garnet can extend to the formational conditions of Sittampundi rocks or high pressure 'eclogites'[10] could have experienced later chemical modification through repeated partial melt extraction or metasomatic overprint[32]. These subsequent effects, if experienced by the studied garnets, add further complications in interpreting the origin of the Sittampundi garnets. Further crystallographic and spectroscopic data are needed to decipher the petrogenetic significance of the Sittampundi garnets.

1. Geller, S., Crystal chemistry of the garnets. *Z. Kristallogr.*, 1967, **125**, 1–47.
2. Winchell, A. N., *Elements of Optical Mineralogy. Part II: Description of Minerals*, John Wiley, New York, 1933, 3rd edn, p. 185.
3. Della Giusta, A., Carbonin, S. and Ottonello, G., Temperature-dependent disorder in a natural Mg–Al–Fe^{2+}–Fe^{3+} spinel. *Mineral. Mag.*, 1996, **60**, 603–616.
4. Ottonello, G., Princivalle, F. and Della Giusta, A., Temperature, composition and fO_2 effects on intersite distribution of Mg and Fe^{2+} in olivines: Experimental evidence and theoretical interpretation. *Phys. Chem. Mineral.*, 1990, **17**, 301–312.

5. Princivalle, F., Della Giusta, A., De Min, A. and Piccirillo, E. M., Crystal chemistry and significance of cation ordering in Mg–Al-rich spinels from high-grade hornfels (Predazzo-Monzoni, NE Italy). *Mineral. Mag.*, 1999, **63**, 257–262.
6. Amthauer, G., Annerstern, H. and Hafner, S. S., The Mössbauer spectrum of ^{57}Fe in silicate garnets. *Z. Kristallogr.*, 1976, **143**, 14–55.
7. Murad, E. and Wagner, F. E., The Mössbauer spectrum of almandine. *Phys. Chem. Miner.*, 1987, **14**, 264–269.
8. Luth, R. W., Virgo, D., Boyd, F. R. and Wood, B. J., Valence and co-ordination of Fe in mantle derived garnets. *Geol. Soc. Am. Abstr. Prog.*, 1988, **20**, A101–A102.
9. Woodland, A. B. and Ross, C. R., A crystallographic and Mössbauer spectroscopy study of $Fe_3^{2+}Al_2Si_3O_{12}$–$Fe_3^{2+}Fe_2^{3+}O_{12}$ (almandine-'skiagite') and $Ca_3Fe_2^{3+}Si_3O_{12}$–$Fe_3^{2+}Fe_2^{3+}Si_3O_{12}$ (andradite-'skiagite') garnet solid solutions. *Phys. Chem. Miner.*, 1994, **21**, 117–132.
10. Subramanium, A. P., Mineralogy and petrology of the Sittampundi complex, Salem district, Madras state, India. *Bull. Geol. Soc. Am.*, 1956, **67**, 317–390.
11. Mitra, S., Bidyananda, M. and Samanta, A. K., Cation distribution in Cr-spinels from the Sittampundi layered complex and their intracrystalline thermodynamics. *Curr. Sci.*, 2006, **90**, 435–439.
12. Bence, A. E. and Albee, A. L., Empirical correction factors for the electron microanalysis of silicates and oxide. *J. Geol.*, 1968, **76**, 382–403.
13. Deer, W. A., Howie, R. A. and Zussman, J., *Rock-forming Minerals: Orthosilicates*. Longman, London, 1982, vol. 1A, p. 919.
14. Yamada, H. and Takahashi, E., Subsolidus phase relations between coexisting garnet and two pyroxenes at 50 to 100 kb in the system CaO–MgO–Al_2O_3–SiO_2. In *Kimberlites II: The Mantle and Crust–Mantle Relationships* (ed. Kornprobst, J.), Elsevier, Amsterdam, 1984, pp. 247–255.
15. Brey, G., Köhler, T. and Nickel, K. G., Geothermobarometry in four phase lherzolites. I: Experimental results from 10 to 60 kb. *J. Petrol.*, 1990, **31**, 1313–1352.
16. Canil, D. and Wie, K., Constraints on the origin of mantle derived from low Ca garnets. *Contrib. Mineral. Petrol.*, 1992, **109**, 421–430.
17. Luth, R. W., Virgo, D., Boyd, F. R. and Wood, B. J., Ferric iron in mantle-derived garnets: Implications for thermobarometry and for the oxidation state of the mantle. *Contrib. Mineral. Petrol.*, 1990, **104**, 56–72.
18. Kan, X., Zhang, E. and Li, Y., The Mössbauer study of pyrope–almandine series and its geological significance. In Abstract 14th IMA Meeting, 1986, p. 137.
19. Evans, B. J. and Sergent Jr, E. W., ^{57}Fe NGR of Fe phases in magnetic cassiterites. I: Chemistry of dodecahedral Ge^{2+} in pyralspite garnets. *Contrib. Mineral. Petrol.*, 1975, **53**, 183–194.
20. Mitra, S., *Applied Mössbauer Spectroscopy: Theory and Practice for Geochemists and Archeologists*, Pergamon Press, Oxford, 1992, p. 400.
21. Woodland, A. B. and Wood, B. J., Electrochemical measurement of the free energy of almandine ($Fe_3Al_2Si_3O_{12}$) garnet. *Geochim. Cosmochim. Acta*, 1989, **53**, 2277–2282.
22. Lager, G. A., Armbruster, Th. and Faber, J., Neutron and X-ray diffraction study of hydrogarnet $Ca_3Al_2(O_4,H_4)_3$. *Am. Mineral.*, 1987, **72**, 756–765.
23. Kohlstedt, D. L., Keppler, H. and Rubie, D. C., Solubility of water in the α-, β- and γ-phases of (Mg, Fe)$_2SiO_4$. *Contrib. Mineral. Petrol.*, 1996, **123**, 345–357.
24. Annadurai, S., Samanta, A. K. and Mitra, S., Infrared spectroscopy in characterisation of metamorphic garnets in relation to other techniques. *Trans. Indian Ceram. Soc.*, 1994, **53**, 109–115.
25. Princivalle, F., Mitra, S., Samanta, A. K., Moon, H. S. and Annadurai, S., Intra-crystalline thermometry and cooling rate of two-pyroxene granulites: Valuation from Mössbauer and X-ray single crystal cation partitioning of Ca-poor and Ca-rich pyroxenes. *Neues Jahrb. Mineral., Monatsh.*, 1999, **1999**, 400–414.
26. Allen, F. M. and Buseck, P. R., XRD, FTIR and TEM studies of optically anisotropic grossular garnets. *Am. Mineral.*, 1988, **73**, 568–584.
27. Kingma, K. J. and Downs, J. W., Crystal structure analysis of a birefringent andradite. *Am. Mineral.*, 1989, **74**, 1307–1316.
28. Akaogi, M. and Akimoto, S., Pyroxene–garnet solid-solution equilibria in the systems $Mg_4Si_4O_{12}$–$Mg_3Al_2Si_3O_{12}$ and $Fe_4Si_4O_{12}$–$Fe_3Al_2Si_3O_{12}$ at high pressure and temperatures. *Phys. Earth Planet. Inter.*, 1977, **15**, 90–106.
29. Nixon, P. H. and Boyd, F. R., Petrogenesis of the granular and sheared ultrabasic nodule suite in kimberlites. In *Lesotho Kimberlites* (ed. Nixon, P. H.), Lesotho National Development Corporation, Maseru, Lesotho, 1973, pp. 48–56.
30. Nixon, P. H., Kimberlite xenoliths and their cratonic setting. In *Mantle Xenoliths* (ed. Nixon, P. H.), John Wiley, New York, 1987, pp. 215–239.
31. Mitra, S., *High Pressure Geochemistry and Mineral Physics*, Elsevier, 2004, p. 1233.
32. Woodland, A. B., Seitz, H.-M., Altherr, R., Marschall, H., Olker, B. and Ludwig, Th., Li abundances in eclogite minerals: A clue to a crustal or mantle origin? *Contrib. Mineral. Petrol.*, 2002, **143**, 587–601.
33. Ryburn, R. J., Råheim, A. and Green, D. H., Determination of the *P*, *T* paths of natural eclogites during metamorphism – Record of subduction. *Lithos*, 1976, **9**, 161–164.

ACKNOWLEDGEMENTS. We thank Prof. H. S. Moon for EMPA data and the Indian Association for the Cultivation of Science and Saha Institute of Nuclear Physics, Kolkata for recording the Mössbauer spectra. Financial support by the University Grants Commission, and the Department of Science and Technology, New Delhi to S.M. and M.B. respectively, is acknowledged. An anonymous reviewer is acknowledged for constructive review.

Received 29 June 2006; revised accepted 16 July 2007

Microbial mat-induced sedimentary structures in the Neoproterozoic Bundi Hill Sandstone, Indargarh area, Rajasthan

S. Kumar* and S. K. Pandey

Centre of Advanced Study in Geology, University of Lucknow, Lucknow 226 007, India

The communication records the development of wrinkle structures and desiccation cracks in the fine-grained Bundi Hill Sandstone belonging to the Neoproterozoic Bhander Group of the Vindhyan Supergroup. The presence of wrinkle structures in the sandstone suggests the role of microbial mats in binding sandy sediments and providing cohesion to the upper surface, which could produce the wrinkle structures and on drying could also produce the mat-related cracks.

*For correspondence. (e-mail: surendra100@hotmail.com)